

**TARGET AND PROJECTILE: MATERIAL EFFECTS ON CRATER EXCAVATION AND GROWTH.**

J.L.B. Anderson<sup>1</sup>, T. Burleson<sup>1</sup>, and M.J. Cintala<sup>2</sup>. <sup>1</sup>Winona State University, Winona, MN (JLAnderson@winona.edu); <sup>2</sup>Code KR, NASA JSC, Houston, TX 77058.

**Introduction:** Scaling relationships<sup>1,2,3</sup> allow the initial conditions of an impact to be related to the excavation flow and final crater size and have proven useful in understanding the various processes that lead to the formation of a planetary-scale crater. In addition, they can be examined and tested through laboratory experiments in which the initial conditions of the impact are known and ejecta kinematics and final crater morphometry are measured directly<sup>4,5</sup>. Current scaling relationships are based on a point-source assumption and treat the target material as a continuous medium; however, in planetary-scale impacts, this may not always be the case. Fragments buried in a megaregolith, for instance, could easily approach or exceed the dimensions of the impactor; rubble-pile asteroids could present similar, if not greater, structural complexity.<sup>6</sup> Experiments allow exploration into the effects of target material properties and projectile deformation style on crater excavation and dimensions. This contribution examines two of these properties: (1) the deformation style of the projectile, ductile (aluminum) or brittle (soda-lime glass) and (2) the grain size of the target material, 0.5-1 mm vs. 1-3 mm sand.

| Table 1. Experiment suites used in this study. |                      |               |
|--|----------------------|---------------|
| Suite  | Projectile           | Target        |
| A  | 3.18 mm glass sphere | 1-3 mm sand   |
| B <sup>7</sup>                                 | 3.18 mm glass sphere | 0.5-1 mm sand |
| C <sup>4</sup>                                 | 4.76 mm Alum sphere  | 1-3 mm sand   |

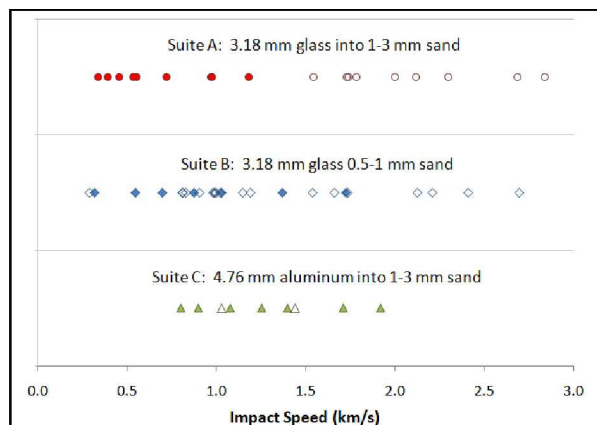


Figure 1. Ranges of impact speeds for the three suites of experiments in this study. Solid symbols are shots which have been used for EVMS analysis. Open symbols are shots which either have not yet been processed (Suite B) or had camera-stability issues which did not allow for EVMS processing (Suite A).

**Data Collection and Experimental Conditions:**

All experiments presented here were performed with the vertical gun in the Experimental Impact Laboratory (EIL) at NASA Johnson Space Center. The ejecta were documented using the Ejection-Velocity Measurement System (EVMS); details regarding the setup and use of the EVMS are given in [4]. Impact speeds ranged between 0.3–2.0 km/s (figure 1); the VIF has a fixed barrel, so the impact angle for all experiments was 90° above the horizontal.

**Data:** Individual ejecta trajectories are measured from the EVMS images and extrapolated back to the target surface, yielding ejection position, speed, and angle data for each particle trajectory observed. In addition, the final crater dimensions for each shot are measured. These data can be analyzed using both crater scaling and ejection-speed scaling relationships.

**Results: Crater-size scaling.** Final crater dimensions have been tied to initial impact conditions through  $\Pi$ -scaling relationships<sup>2,3</sup> which infer that a single parameter  $\alpha$  is related to the slope of the  $\Pi_R$  vs.  $\Pi_2$  relationship. (This parameter is also related to the exponent in the ejection-speed scaling relationships, as discussed below.) A fit to all the available shots from the three suites yields a value for  $\alpha$  of 0.471 (figure 2). Values of  $\alpha$  obtained through crater-size scaling of each individual suite are given in Table 2.

| Table 2. Crater-scaling results for each suite. |          |       |
|---|----------|-------|
|   | $\alpha$ | $R^2$ |
| Suite A   | 0.471    | 0.968 |
| Suite B   | 0.468    | 0.934 |
| Suite C   | 0.450    | 0.967 |
| All Suites                                      | 0.471    | 0.950 |

**Ejection-speed scaling.** The scaled ejection speed is related to the scaled ejection position by a power law whose exponent  $e_x$  is a function of  $\alpha$ . This exponent and the derived value of  $\alpha$  was calculated for each shot in the three series and is plotted in figure 3. A few of the values of  $\alpha$  for the two glass suites fall above the predicted theoretical maximum.

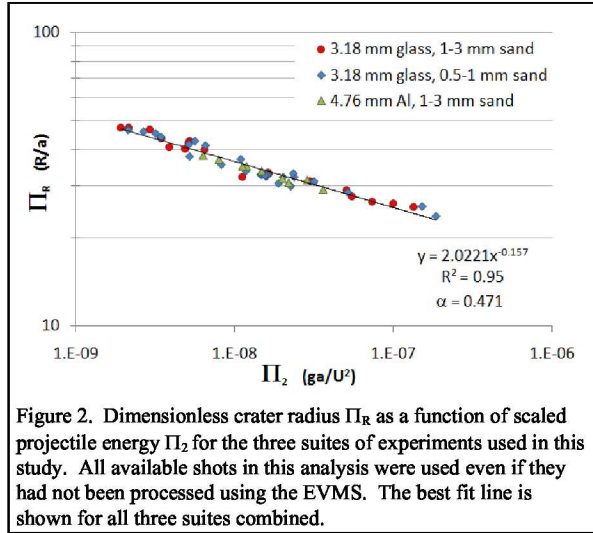


Figure 2. Dimensionless crater radius  $\Pi_R$  as a function of scaled projectile energy  $\Pi_2$  for the three suites of experiments used in this study. All available shots in this analysis were used even if they had not been processed using the EVMS. The best fit line is shown for all three suites combined.

**Discussion:** As was the case with Suites B<sup>7</sup> and C<sup>4</sup>, the value of  $\alpha$  derived from crater-size scaling differed considerably from that derived from the ejection-speed scaling for suite A. In all cases, the  $\alpha$  from crater-size scaling is less than  $\alpha$  derived from the ejection-speed scaling and closer to the theoretical minimum. It is interesting to note that a separate suite of experiments with larger (6.35 mm) aluminum projectiles into a finer-grained sand (mean grain size of 0.55 mm) at similar impact speeds (near 1.0 km/s) yielded essentially identical values of  $\alpha$  as determined from the crater-size scaling and ejection-speed scaling relationships.<sup>7,8</sup> It is possible that the relative coarseness of the target material in the experiments presented here violated the point-source assumption inherent to the scaling relationships.<sup>9</sup> This and other possibilities will continue to be examined through additional experiments.

**Target material grain size.** From this initial study, it does not appear that the difference in grain size between suites A and B plays a significant role in either the crater-size scaling or the ejection-speed scaling since the values of  $\alpha$  are generally indistinguishable in both analyses. It may be that the finer-grained targets show a slightly smaller spread in  $\alpha$  as derived from ejection-speed scaling than the coarser-grained targets (figure 3). A number of shots in Suite B, however, have yet to be processed, so this can only be considered a suggestion until completion of the additional analyses.

**Ductile vs. brittle deformation of the projectile.** The aluminum and glass suites differ in  $\alpha$  as derived from crater-size scaling. As the aluminum projectile experiences ductile deformation and therefore pene-

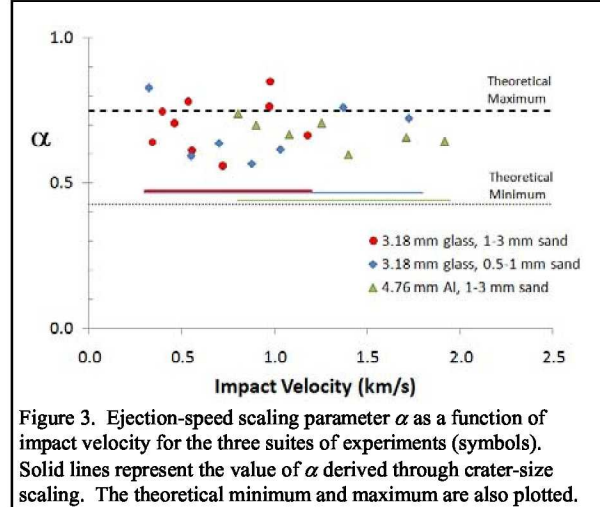


Figure 3. Ejection-speed scaling parameter  $\alpha$  as a function of impact velocity for the three suites of experiments (symbols). Solid lines represent the value of  $\alpha$  derived through crater-size scaling. The theoretical minimum and maximum are also plotted.

trates deeper into the target material, it is reasonable that the parameter  $\alpha$  is lower, as smaller values imply a larger role for momentum in crater growth. The glass projectiles shatter as they deposit their energy close to the target surface.<sup>10</sup> It is notable, however, that the range of  $\alpha$  derived through ejection-speed scaling for the glass and aluminum experiments is very nearly the same for all three suites, but different from the values derived through the crater-size scaling. The  $\alpha$  values for the aluminum suite are less scattered (and potentially follow a trend with increasing impact speed) than the glass suites. This may also be due to the deformation style of the projectile; the glass projectiles shatter near the target surface and may generate more chaotic ejecta kinematics than the aluminum which delivers its energy more deeply into the target. Further analysis of these shots as well as additional experiment suites will help address these questions.

**Conclusions:** It is clear that deformation style and target material properties play roles in crater excavation. Further experimental suites are planned to address the issues raised here and expand the parameter space of this study.

**References:** <sup>1</sup>Chabai A.J. (1965) *JGR* 70, 5075. <sup>2</sup>Holsapple K.A. and Schmidt R.M. (1982) *JGR* 87, 1849. <sup>3</sup>Housen *et al.* (1983) *JGR* 88, 2485. <sup>4</sup>Cintala M.J. *et al.* (1999) *MAPS* 34, 605. <sup>5</sup>Anderson, J.L.B. *et al.* (2003) *JGR* 108, doi:10.1029/2003JE002075. <sup>6</sup>Fujiwara, A. *et al.* (2006) *Science* 312, 1330. <sup>7</sup>Anderson, J.L.B. *et al.* (2007) *LPSC* 38, #2266. <sup>8</sup>Anderson, J.L.B., unpublished data. <sup>9</sup>Barnouin-Jha O.S. *et al.* (2005) *LPSC* 36, #1585. <sup>10</sup>Anderson, J.L.B. *et al.* (2004) *MAPS* 39, 303.